JOURNAL OF MATERIALS SCIENCE 33 (1998) 3361–3370

Influence of rhenium on the microstructures and mechanical properties of a mechanically alloyed oxide dispersion-strengthened nickel-base superalloy

H. S. KO*, K. W. PAIK
Department of Materials Science and Engineering, Korea Advanced Institute of Science and Technology, Kusong-dong, Yusong-gu, Taejon 305-701, Korea
E-mail: kwpaik@sorak.kaist.ac.kr

L. J. PARK
Agency for Defense Development, Yusong P.O. Box 35-1, Taejon 305-600, Korea

Y. G. KIM
Handong University, Namsong-li, Heunghae-eup, Pohang-si, Kyungsangbook-do 795-940, Korea

J. H. TUNDERMANN
Inco Alloys International Huntington, WV 25705, USA

The influence of a 3 wt% Re addition on the creep strength and microstructure of a mechanically alloyed and oxide dispersion-strengthened nickel-base superalloy was investigated. Two alloys, Ni–8Cr–6.5Al–6W–3Ta–1.5Mo–6Co–1Ti–3Re–0.15Zr–0.05C–0.01B–$0.9Y_2O_3$ (3Re alloy) and a non-rhenium containing (0Re) alloy were prepared for this study.

The 3Re alloy showed two-fold improvement in creep life compared with that of 0Re alloy, presumably due to a change in the mode of the precipitate–dislocation interaction. For the 3Re alloy, finer, more cuboidal and aligned γ' precipitates are formed, which force the mobile dislocations at the γ–γ' interfaces to cut precipitates in order to proceed. Shearing of precipitates is evinced by the existence of stacking faults and results in an increase of creep strength. In contrast, lower creep strength was observed for 0Re alloy because a dislocation looping mode is dominant with coarser and more irregularly shaped γ' precipitates present in this alloy. Another possible explanation for an improved creep strength of 3Re alloy is related to the tangled dislocation structure formed by the interaction between glide dislocation and interfacial dislocation, which also acts as an effective barrier for further glide dislocation motion. A 3 wt% Re addition significantly retards γ' coarsening kinetics. Rhenium acts as a rate-controlling species upon the volume diffusion-controlled coarsening process because it is a heavy element and also it almost solely partitions to the γ matrix. X-ray diffraction experiments showed that the magnitude of the lattice mismatch between γ and γ' increased with the 3 wt% Re addition from 0% to -0.26% at room temperature. Increased lattice mismatch for 3Re alloy causes the formation of more aligned and cuboidal γ' precipitates rather than random and odd-shaped γ' precipitates for 0Re alloy, and it also accelerates the coalescence between cuboidal γ' precipitates. © *1998 Kluwer Academic Publishers*

1. Introduction

Advances in the development of high-temperature alloys have been accomplished through incorporation of inert yttrium oxide dispersoids into a high volume fraction (> 60 vol%) γ' precipitation strengthened nickel-base superalloy by the mechanical alloying process. Inconel (trademark of the Inco family of companies) alloy MA 6000, designed by Inco Alloys International, was the first commercial alloy developed along these lines [1]. However, the strength of alloy MA 6000 at intermediate temperatures of 750–950 °C is inferior to those of single-crystal, nickel-base superalloys such as PWA 1480 and CMSX-2 [2]. Numerous attempts have been made to develop new

*Auhor to whom all correspondence should be addressed.

mechanically alloyed oxide dispersion-strengthened (MA ODS) nickel-base superalloys whose strengthens are comparable to single-crystal superalloys. These attempts resulted in the development of alloy 92, which satisfied the need for intermediate-and high-temperature strength at the same time.

The major modification of alloy 92 compared to alloy MA 6000 is the addition of the refractory element rhenium as is the case for several modern single-crystal superalloys such as PWA 1484 and CMSX-4. Rhenium is known to be a potent strengthener of nickel-base superalloys under creep conditions. The works presented prior to 1990, including limited data regarding rhenium additions to some alloy systems [3,4], did not explain the observed strengthening mechanism.

The purpose of this study was to investigate the effect of a 3 wt % Re addition on the microstructures and the mechanical properties of the alloys, which included the effect of the rhenium addition on γ' coarsening kinetics and γ–γ' lattice mismatch. Alterations in the γ–γ' lattice mismatch and coarsening rate of γ' precipitate due to the rhenium addition were expected to induce morphological change of γ' particles at various stages of heat treatment. On the basis of the γ' morphological change, creep rupture behaviour at intermediate temperature, typically 760 °C, was also examined.

2. Experimental procedures

Two different MA ODS nickel-base superalloys, alloy 92 and a rhenium-free version of alloy 92, were prepared for this study at Inco Alloys International. For ease of comparison, alloy 92 and the other alloy were called 3Re alloy and 0Re alloy, respectively. The compositions of these alloys were determined by the inductively coupled plasma spectroscopy (ICPS) method and are listed in Table I.

Elemental and master alloy powders were mechanically alloyed in an attritor ball mill. The mechanical alloyed powders were packed into mild steel cans and subsequently evacuated and sealed. The sealed can was extruded into 1.8 cm diameter bars at 1175 °C using an extrusion ratio of 17 : 1.

In order to investigate the effect of the rhenium addition on γ' coarsening behaviour, as-extruded specimens were isothermally aged at temperatures between 1000 and 1200 °C for times of up to 72 h. These specimens were rapidly water-quenched upon completion of the isothermal ageing treatments. After the ageing treatments, the specimens were metallographically polished and electro-etched at 0.25A cm^{-1} for 3–4 min in a fresh solution of 17 ml H_2O + 2 ml HNO_3 + 1 ml CH_3COOH. Scanning electron microscopy (SEM) was used to examine the γ–γ' microstructures. Quantitative measurements of the γ' size were made directly on the scanning electron micrographs using Bioscan® OPTIMAS™ image analyser system. The mean edge length of the γ' particles was determined from the square root of the mean area of γ' particle which was calculated using the image analyser system.

X-ray diffraction using CuK_α radiation was employed to measure the lattice mismatch between γ and γ' phases which affects the shape of the γ' precipitates. The magnitude of lattice mismatch was determined from the difference in lattice parameters calculated from the $(2\,2\,0)_{\gamma,\gamma'}$ peaks. In cases where the γ and γ' peaks overlapped, the X-ray peaks were resolved with the peak fitting technique using a Lorentzian function. A high-temperature attachment was used to acquire the $(2\,2\,0)_{\gamma,\gamma'}$ peaks from 25–850 °C. On occasion, the specimen holder became slightly misaligned during heating. This resulted in a loss of total diffracted intensity and resolution of the γ and γ' peaks. The maintenance of good alignment was considered to be an important factor controlling the precision of the lattice parameter measurements.

To prepare creep-test specimens, material in the as-extruded condition was zone annealed at a hot-zone temperature of 1290 °C with constant furnace travel speed of 55 mm h^{-1}. Zone annealing is a heat treatment employed to produce a coarse elongated grain structure, which is indispensable to high-temperature performance. The specimens were given the following three-stage heat treatment, conventionally referred to as γ' heat treatment. The objective of this treatment was to solution-treat coarse γ' precipitates formed after zone annealing and then to produce the morphology with fine and regularly shaped γ' precipitates, which is optimum for mechanical properties. 1280 °C/2 h/AC + 950 °C/2 h/AC + 850 °C/24 h/AC (AC = air cooled).

The specimens for creep test were machined with gauge diameter of 4.5 mm and gauge length of 18 mm after γ' heat treatment. Constant-load creep tests were conducted in air at 760 °C and two stress levels of 650 and 600 MPa, with the tensile axis parallel to the extrusion direction. Transmission electron microscopy (TEM) was employed to observe the effect of γ' morphology on the γ' particle–dislocation interaction mode. Thin-foil TEM samples taken from creep-ruptured surfaces were jet polished in a twin-jet electro-polisher operating at 30 V in a 9 : 1 mixture of ethanol and perchloric acid whose temperature was close to − 50 °C.

TABLE I Chemical compositions of alloys (wt %)

Alloy		Ni	Co	Cr	Al	Ti	Ta	Mo	W	Re	B	C	Zr	Y_2O_3
3Re Alloy	Aim	Bal.	6	8	6.5	1	3	1.5	6	3	0.01	0.05	0.15	0.9
	Analysed	63.87	6.7	8.61	6.19	0.97	2.9	1.22	6.31	2.21	0.015	0.05	0.134	0.66
0Re Alloy	Aim	Bal.	6	8	6.5	1	3	1.5	6	–	0.01	0.05	0.15	0.9
	Analysed	65.71	6.78	8.84	6.15	1.02	2.99	1.25	6.44	0.015	0.01	0.05	0.15	0.673

3. Results and discussion

3.1. Effect of rhenium on γ′ morphology

3.1.1. Coarsening rate of γ′ precipitate

The effect of the 3 wt % Re addition on γ′ precipitate coarsening was examined by comparing mean γ′ precipitate sizes in 3Re and 0Re alloys at various ageing temperatures and times. Ageing temperatures and times were varied from 1000–1200 °C and up to 72 h before massive coalescence occurred. Figs 1 and 2 show γ′ coarsening behaviour as ageing time increases at 1100 °C. γ′ precipitates in 3Re alloy were much finer than those in 0Re alloy at the same ageing times. Mean γ′ particle was derived from the square root of mean γ′ particle area, which was calculated using Bioscan® OPTIMAS™ image analyser system. Fig. 3 shows the mean particle size as a function of time for all ageing temperatures. A linear relationship was observed between the cube of average particle size and ageing time, expressed as

$$(\bar{a}/2)^3 - (\bar{a}_0/2)^3 = kt \qquad (1)$$

where $\bar{a}$ is the mean γ′ particle size, $\bar{a}_0$ the initial mean γ′ particle size, k is the coarsening rate constant, and t is the ageing time at given temperature. The initial mean γ′ size, $\bar{a}_0$, has been subtracted from the ordinate values of each alloy to take into account the small variations in initial particle size which resulted from slight variations in quenching conditions. The linear relationship indicates that coarsening of γ′ precipitate follows the diffusion-controlled kinetics theory which was originally suggested by Lifshitz and Slyozov [5] and by Wagner [6]. It was also evident that γ′ particles coarsened more rapidly as the ageing temperature increased.

Comparing Fig. 3a and b, it was found that the 3 wt % Re addition significantly retarded the γ′ coarsening kinetics because rhenium increased the activation energy for particle coarsening. A simple model can be suggested to explain the result at first. Because the partitioning ratio of rhenium, $a_{\text{Re in }\gamma}/a_{\text{Re in }\gamma'}$, was found to be about 4.3 or higher by wavelength dispersive spectroscopy (WDS) analysis, it is necessary for rhenium to diffuse from the high rhenium-containing γ phase to allow the growth of the γ′ phase. During a diffusion-controlled process, the diffusivity of rhenium can be regarded as small, because rhenium is a much heavier element than nickel. Unfortunately, no rhenium diffusion data in nickel are available. Therefore, tungsten was considered to have similar diffusivity to rhenium due to its similar size and mass. The activation energy, Q, and vibrational component, D_0, for tungsten in nickel are 299 kJ mol^{-1} and 2×10^{-4} m^2 s^{-1}, respectively, and the self-diffusion of nickel corresponds 284 kJ mol^{-1} and 1.9×10^{-4} m^2 s^{-1} for that as determined by radioactive tracer diffusion studies [7]. At 1000 K, the self-diffusion coefficient, $D_{\text{Ni-Ni}}$, is an order of magnitude greater than $D_{\text{W-Ni}}$. Therefore, it is confidently expected that the rhenium diffusion from the γ–γ′ interface limits the diffusion-controlled γ′ particle coarsening process.

To verify the explanation suggested above, the effect of rhenium addition on the activation energy for particle coarsening was quantitatively investigated. It is well known that a plot of $\ln k$ versus $1/T$ gives an activation energy for the coarsening process which should be approximately equal to the activation energy for diffusion of the solute in the matrix [8]. The activation energies for the coarsening of two alloys were found to be 191 and 262 kJ mol for 0Re alloy and 3Re alloy, respectively, as shown in Fig. 4. In other words, the activation energy for coarsening increased by 38% upon the 3 wt % Re addition, which is very consistent with the previous results [4].

3.1.2. Particle shape of γ′ precipitate

It is well known that the morphology of coherent precipitate in two-phase alloys is strongly influenced by the elastic strain energy associated with the lattice mismatch between precipitate and matrix structure [9–11]. The elastic strain energy depends on the shape, habit and configuration of the precipitates as well as on their volume. So the shape of a coherent particle is determined by the balance between interfacial energy and elastic strain energy. For an alloy of small lattice mismatch between matrix and particle, a spherical (or round on a sectioning plane) shaped γ′ precipitate is formed according to the interfacial energy minimization criterion. In contrast, for an alloy of large lattice mismatch, an elastically favoured cuboidal γ′ precipitate is formed. Because interfacial energy and elastic strain energy are proportional to the square and the cube of the particle radius, respectively, an alloy of fixed lattice mismatch, δ, experiences morphological transition of the precipitate from sphere to cuboid.

The effect of rhenium addition on lattice mismatch was investigated using X-ray diffraction. Figs 5 and 6 show typical diffraction peaks taken from the {2 2 0} plane of 3Re alloy and 0Re alloy after γ′ heat treatment. As can be seen in Fig. 5, diffraction peaks for 3Re alloy can be resolved into two peaks from both γ and γ′ phases. But the lower lattice mismatch of 0Re alloy resulted in complete overlap of the γ and γ′ peaks so that peak separation was barely possible. To measure the lattice parameter of each phase, the peak separation was accomplished by a peak-fitting technique based on Lorentzian function. The lattice mismatch can be calculated using the following equation [12]

$$\delta = \frac{2(a_{\gamma'} - a_\gamma)}{a_{\gamma'} + a_\gamma} \qquad (2)$$

where $a_{\gamma'}$ is the lattice parameter of γ′ and a_γ is the lattice parameter of γ.

The lattice mismatches of two alloys are shown as a function of temperature in Fig. 7. All of the lattice mismatches of 0Re alloy were found to be below the resolution limit of the measurement technique and were regarded as 0 in magnitude at all test temperatures. The room-temperature lattice mismatch increased from 0 to −0.26% with 3 wt % Re addition

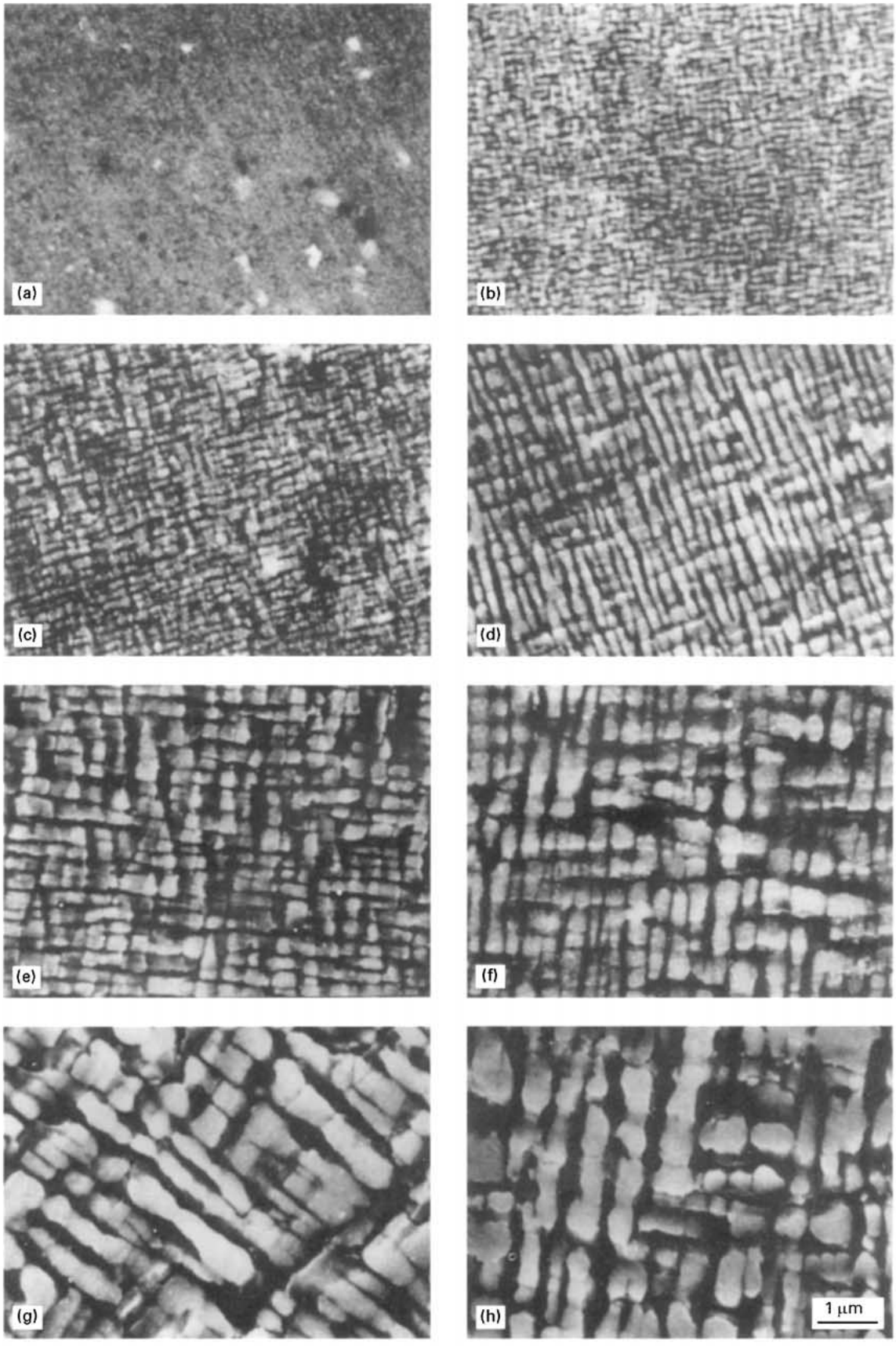

Figure 1 Coarsening γ′ cubes for 3Re alloy at 1100 °C after solid solution treatment. (a) As-solution treated, (b) 10 min, (c) 30 min, (d) 2 h, (e) 5 h, (f) 10 h, (g) 24 h, (h) 48 h.

and more at higher temperatures, because the larger rhenium atom compared to nickel almost solely partitions to γ matrix, as already evinced by WDS analysis. The lattice parameter of the γ matrix increased more with increasing temperature than that of the γ′ particle. As a result, the lattice mismatch of 3Re alloy became more negative at higher temperatures. It seems that the deviation of lattice mismatch at 850 °C is associated with the precipitation of Ni_3Mo in this temperature range, as already reported by other investigators [12].

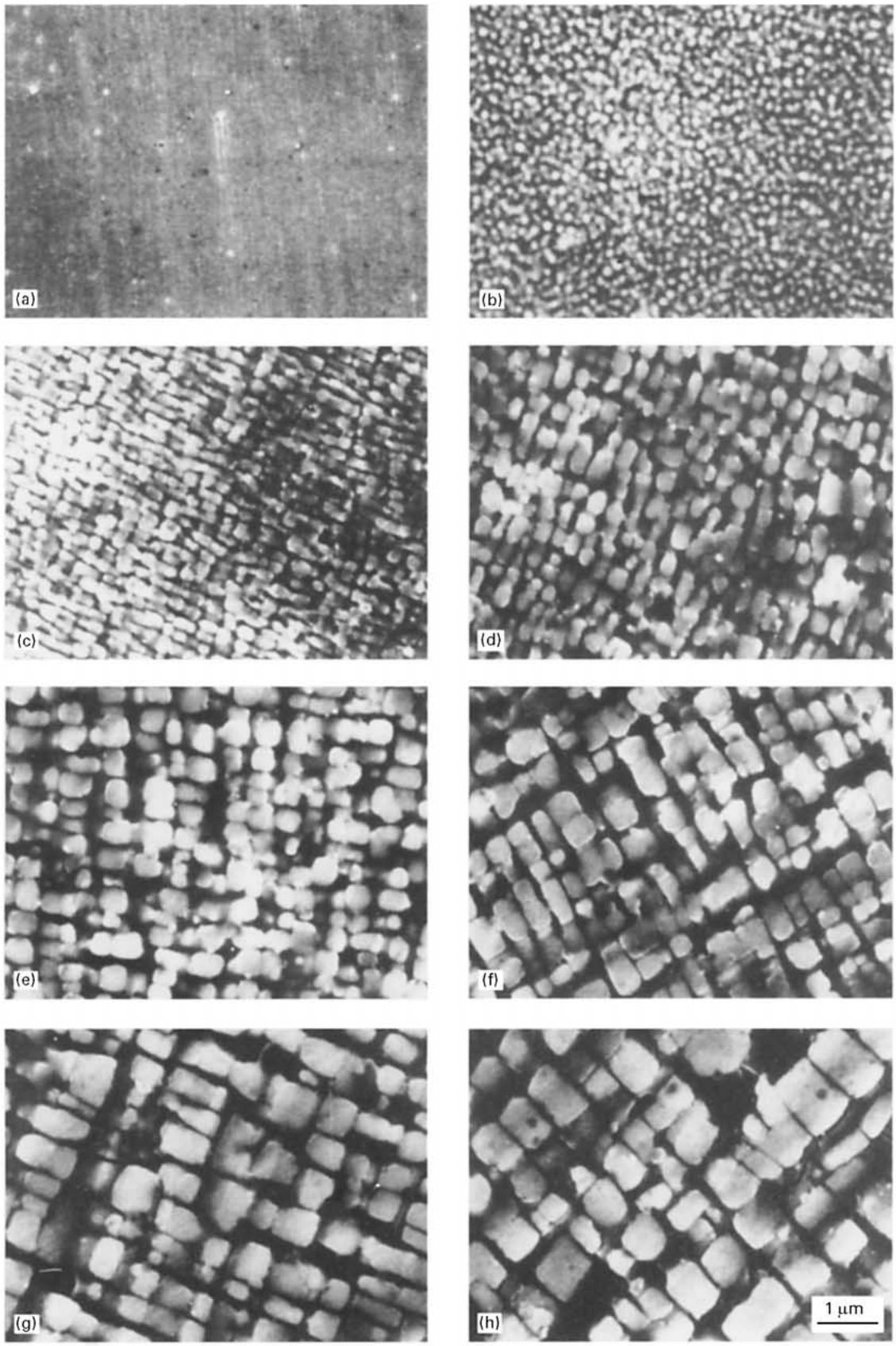

Figure 2 Coarsening γ′ cubes for 0Re alloy at 1100 °C after solid solution treatment. (a) As-solution treated, (b) 10 min, (c) 30 min, (d) 2 h, (e) 5 h, (f) 10 h, (g) 24 h, (h) 48 h.

The increased lattice mismatch caused by the rhenium addition resulted in the different γ′ morphology upon isothermal ageing. Using the equations [13]

$$\text{elastic strain energy} = a\delta^2 V \quad (3)$$

$$\text{interfacial energy} = b\gamma^* r^2 \quad (4)$$

$$\text{critical size, } r_0 = \frac{c\gamma^*}{\delta^2} \quad (5)$$

where δ is the lattice mismatch between γ and γ′, γ^* the interfacial energy between γ and γ′, V the volume of the γ′ particle, r the radius of a γ′ particle, and a, b, c are dimensional constants.

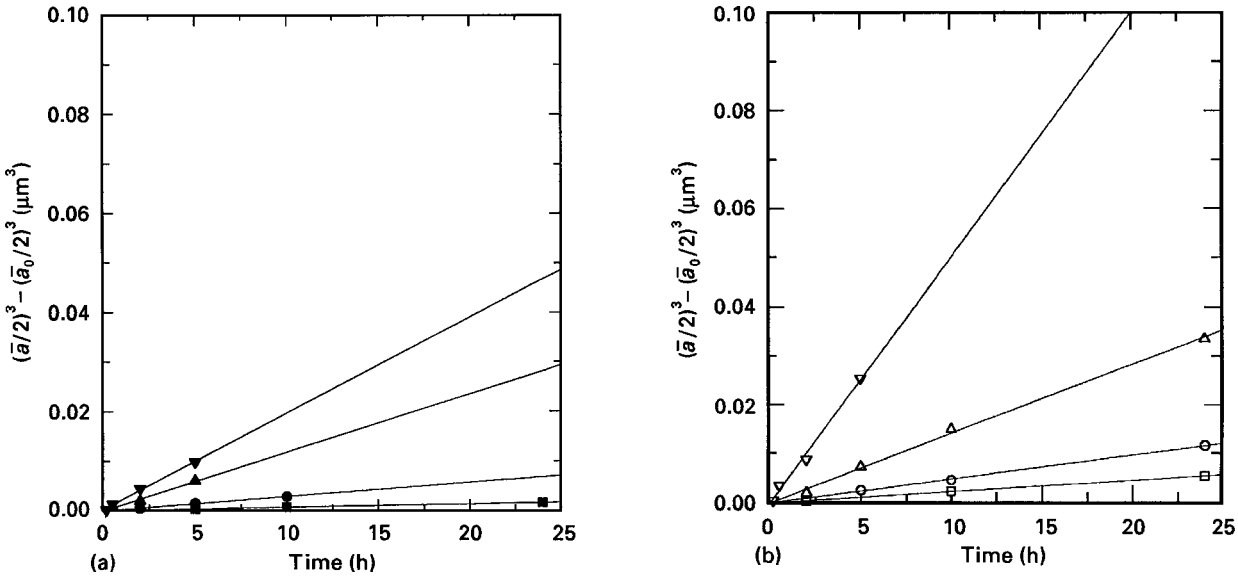

Figure 3 Plot of (half of the mean particle edge length)^3 against time for, (a) 3Re alloy, (b) 0Re alloy. (■, □) 1000 °C, (●, ○) 1100 °C, (▲, △) 1150 °C, (▼, ▽) 1200 °C.

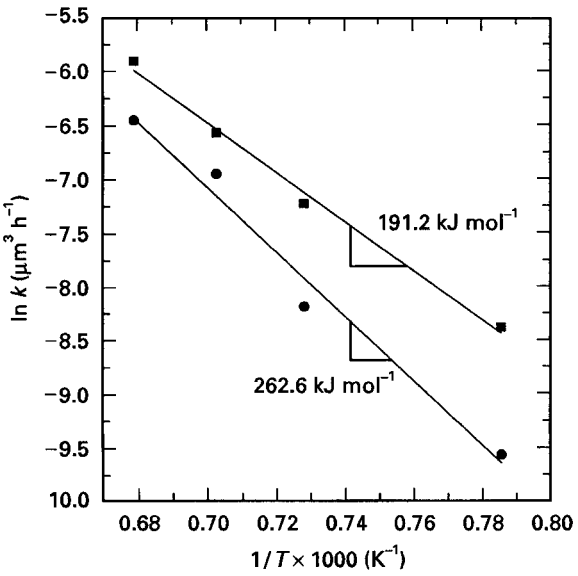

Figure 4 Plot of the logarithm of the rate constants in Fig. 3 against the reciprocal of the abosulte temperature: (■) 0Re alloy, (●) 3Re alloy.

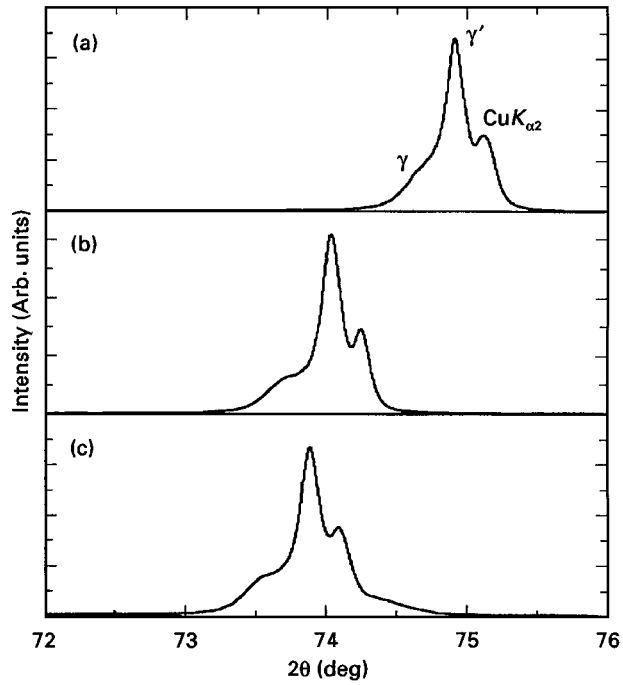

Figure 5 {220} X-ray diffraction peaks of 3Re alloy at (a) RT, (b) 750 °C, (c) 850 °C.

A schematic diagram, Fig. 8, can be developed showing the effect of lattice mismatch on the critical particle size where the interfacial and elastic strain energies are in balance. Therefore, 3Re alloy with the larger lattice mismatch has a smaller critical particle size, r_{c3}, where particle shape transition from sphere to cuboid occurs. As already observed from the results of isothermal ageing at 1100 °C, the precipitate shape transition from sphere to cuboid for 3Re alloy occurred within approximately 30 min to form very fine precipitates. For 0Re alloy, however, coarse and cuboidal precipitates were formed after 10 h.

After a prolonged ageing time, massive coalescence between coarse cuboidal γ′ precipitates occurred to form plate-shaped γ′. The driving force of this coalescence stems from the reduction in elastic strain energy accomplished by annihilating strain fields surrounding each γ′ precipitate, which is similar to the case for the shape transition. It has also been suggested [14,15] that the onset of the formation of plate-shaped γ′ is associated with the loss of coherency between precipitate and matrix. For 3Re alloy which has higher elastic strain fields due to larger lattice mismatch between γ and γ′, γ′ plates formed by coalescence between γ′ cuboids were observed after ageing treatment for 24 h at 1100 °C, while for 0Re alloy, the discrete and coarse cuboidal γ′ particles were still observed after 48 h at 1100 °C.

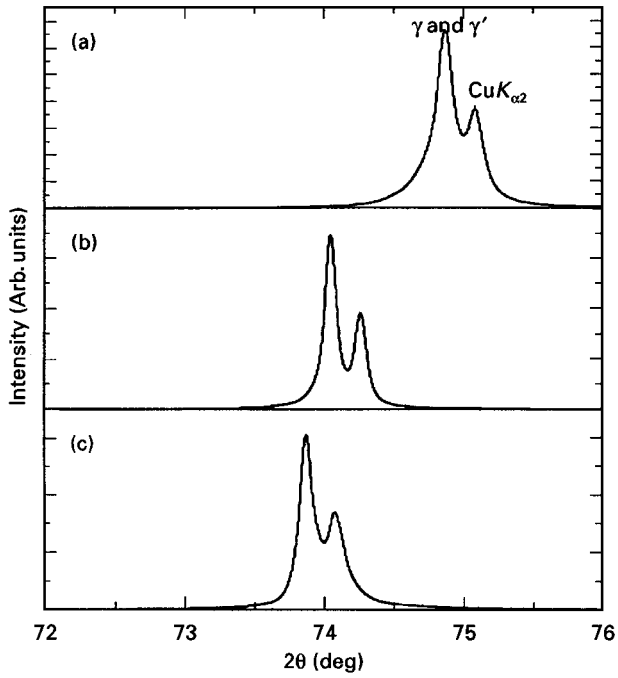

Figure 6 {220} X-ray diffraction peaks of 0Re alloy at (a) RT, (b) 750 °C, (c) 850 °C.

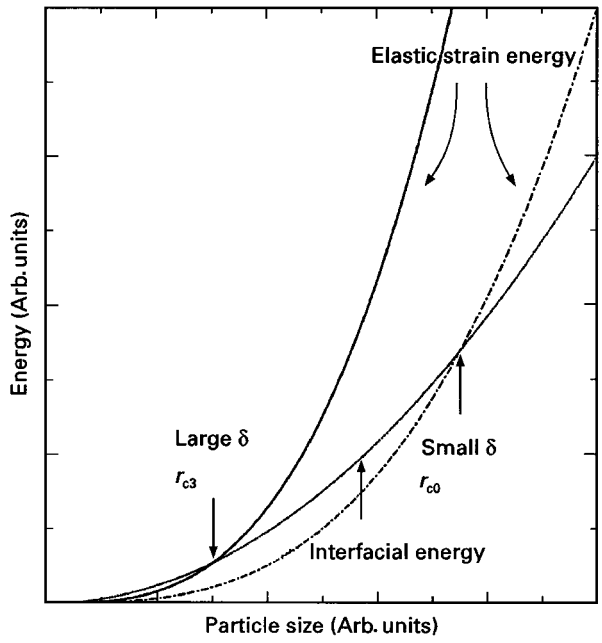

Figure 8 Relation between the lattice mismatch and the critical particle size where the interfacial energy and elastic energy are in balance: (——) 3Re alloy, (– · –) 0Re alloy.

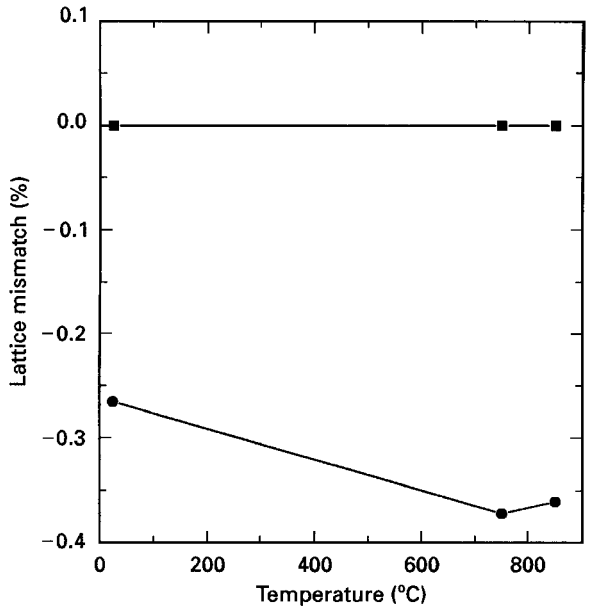

Figure 7 Temperature dependence of lattice mismatch of γ and γ′ phases: (●) 3Re alloy, (■) 0Re alloy.

3.2. Effect of the 3 wt % Re addition on creep strength at intermediate temperature

3.2.1. Microstructure after γ′ heat treatment for a creep-test specimen

The typical microstructure of each alloy after the γ′ heat treatment is shown in Fig. 9. For 3Re alloy, finer, more cuboidal and aligned γ′ precipitates were formed after γ′ heat treatment while coarser and more irregularly shaped γ′ precipitates in 0Re alloy. This is consistent with the observation of the effect of isothermal ageing at 1100 °C. Because alignment of particles is caused by elastic interaction, the driving force for alignment is proportional to the elastic strain energy and the lattice mismatch between γ and γ′. Therefore, more pronounced alignment of γ′ particles was found for 3Re alloy with higher lattice mismatch, while a rather random distribution of γ′ particles was observed for 0Re alloy.

3.2.2. Creep test results

To investigate the effect of the 3 wt % Re addition on morphological changes of the γ′ precipitates and on mechanical properties of the alloys, tensile creep tests were run at 760 °C. The load condition was fixed to be two stress levels of 600 and 650 MPa. The results of these creep tests are given in Table II, and typical creep curves corresponding to the two alloys are shown in Fig. 10. The time to creep rupture of 3Re alloy was twice as long as that of 0Re alloy at the tensile stress of 650 MPa and more than twice at 600 MPa. The steady state creep rates decreased by an order of magnitude with 3 wt % Re addition.

The strengthening of nickel-base superalloys containing γ′ precipitates of 60–70 vol % is mainly provided by the precipitate in the intermediate temperature region of 750–950 °C. Although the oxides in the conventional ODS alloys improve the high-temperature capability of those alloys, they have little effect on the strength near 760 °C owing to the quite low volume fraction of the oxide compared to that of γ′ precipitate.

The effectiveness γ′ precipitate in strengthening nickel-base superalloys is related to the size, shape, distribution, and volume fraction of γ′ precipitates [16]. Among these, γ′ volume fraction was not found to be largely influenced by the 3 wt % Re addition. Consequently, the size, shape, and distribution of γ′ precipitates must be considered in order to understand the difference in creep properties between 3Re

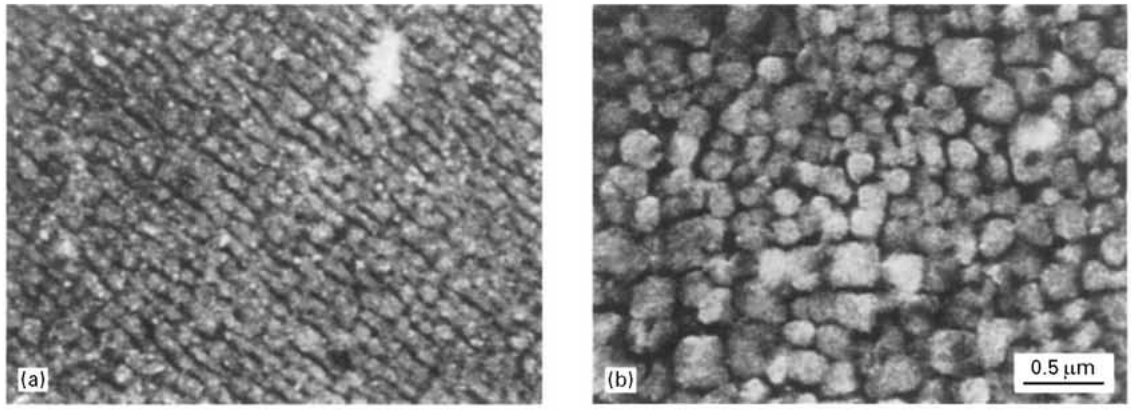

Figure 9 The microstructures after γ′ heat treatment: (a) 3Re alloy, (b) 0Re alloy.

TABLE II Results of creep test at two stress levels

Alloy	3Re Alloy		0Re alloy	
	650 MPa	600 MPa	650 MPa	600 MPa
Time to rupture (h)	98.3	257.6	48.9	98.3
Total elongation (%)	3.47	1.07	2.63	1.68
Steady state creep rate (s^{-1})	6.075×10^{-6}	5.944×10^{-7}	1.471×10^{-5}	6.075×10^{-6}

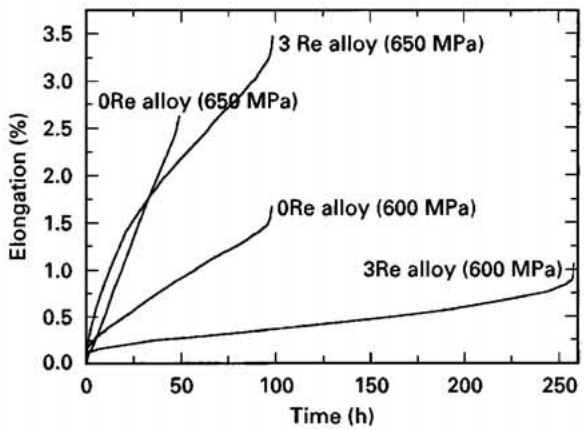

Figure 10 Creep curves for 3Re and 0Re alloys at 760 °C and 650/600 MPa.

and 0Re alloys. The two-fold improvement in creep strength exhibited by 3Re alloy compared to 0Re alloy can be explained in terms of the change of the precipitate–dislocation interaction mode induced by γ′ morphology change, as can be seen in Fig. 9.

The TEM observations shown in Fig. 11, for the samples creep ruptured at 760 °C and 650 MPa, show the typical dislocation configurations. There are two obvious differences between the dislocation structures of the alloys which are closely related to the increase in creep strength for 3Re alloy. One difference involves many stacking faults, which are only observed in γ′ precipitates for 3Re alloy. The other is that the dislocation density for 3Re alloy is significantly higher than that for 0Re alloy.

Firstly, γ′ precipitate shearing accompanied by stacking faults strongly depends on the size of the γ′ particle. Fig. 11a shows the stacking faults in the precipitates on {1 1 1}-type planes. The nature of such intrinsic–extrinsic stacking faults was completely identified by other researchers [17,18]. For the finer γ′ precipitate in 3Re alloy, the mobile dislocations at the γ– γ′ interface must cut through the precipitate in order to proceed. Shearing of a precipitate by $\{1\,1\,1\}\langle 1\,1\,2\rangle$ slip accompanied with the formation of stacking fault resulted in an increase of creep strength. However, Orowan dislocation looping, which is responsible for lower creep strength, was found in 0Re alloy having coarser γ′ precipitate, as seen in Fig. 11b.

Secondly, it is suggested that the particle–dislocation interaction mode also depends on the shape of the γ′ particle. The following line tension consideration indicates that shearing at the corners of an array of cuboidal γ′ particles will be more probable than at spherical or more irregularly shaped γ′ particles. Schematic dislocation configurations observed in the {1 1 1} planes in both γ′ morphologies of cuboidal and spherical precipitates are shown in Fig. 12. The $a/2\langle 1\,1\,0\rangle$ dislocations gliding on the {1 1 1} planes are arrested at the γ– γ′ interfaces. The cuboidal precipitate of 3Re alloy appears as triangles with rounded corners and the radius of curvature of the dislocation around the corner of the precipitate is obviously small. But in the case of 0Re alloy having spherical or more rounded γ′ precipitates, the cross-section of the particle in the {1 1 1} plane is close to a sphere and the radius of curvature of the dislocation is as large as the particle size.

According to Copley and Kear [19], a force due to the line tension of a curved dislocation acts normal to the dislocation and towards its centre of curvature. This force plays a key role in pushing the dislocation

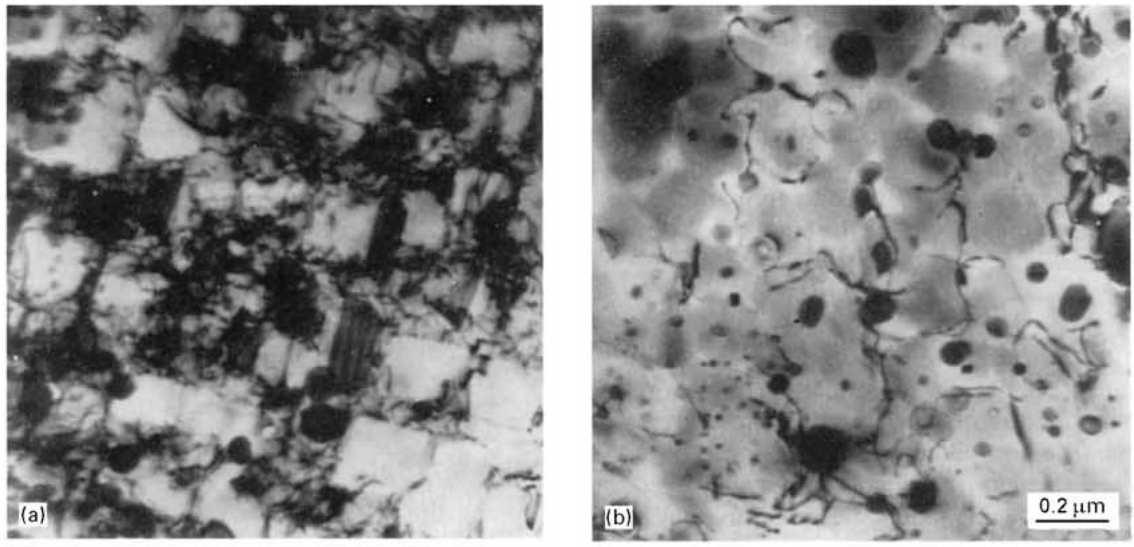

Figure 11 TEM observations of transverse sections of creep ruptured samples tested at 760 °C/650 MPa. (a) 3Re alloy (time to rupture = 98.3 h), (b) 0Re alloy (time to rupture = 48.9 h). The thin foil normals are [0 0 1].

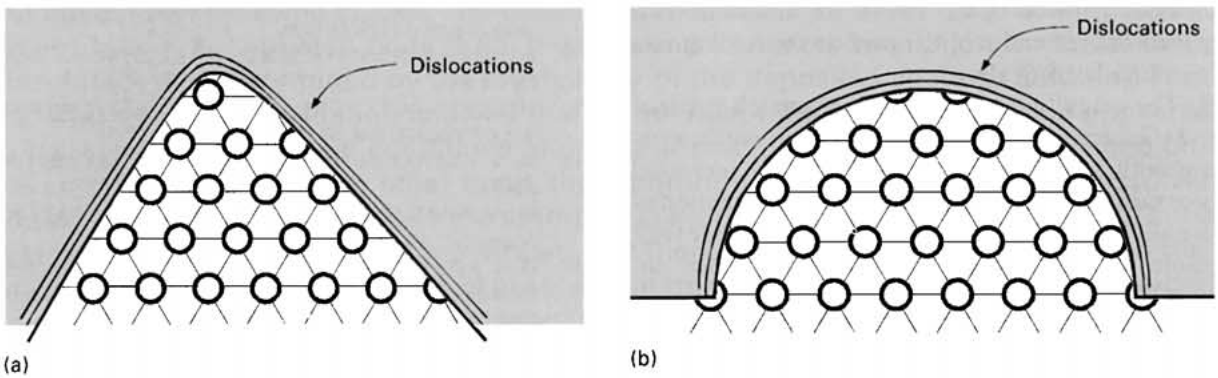

Figure 12 Dislocation configurations on the {1 1 1}-type planes around (a) cuboidal, (b) spherical γ′ precipitates.

into the precipitate and is given by

$$F = \phi/r_0 \quad (6)$$

where ϕ is the line tension and r_0 the radius of curvature of the dislocation. The force F will increase with decreasing radius of curvature and hence the dislocation penetration in the {1 1 1} planes will become more probable at the corner of the cuboidal precipitates than in the nearly spherical particle. Therefore, the higher pushing force exerted to the dislocation at the corner of the cuboidal γ′ precipitate enhances the deformation mechanism by the particle shearing with the {1 1 1}⟨1 1 2⟩ slip system, which is responsible for the improved creep strength of 3Re alloy.

Furthermore, the higher dislocation density may also be responsible for the improved creep rupture strength of 3Re alloy related to the coherency strengthening of the γ–γ′ interface induced by the lattice mismatch between two phases. Several studies on a variety of precipitation hardenable alloy systems have presented unequivocal experimental evidence supporting coherency strain strengthening as a major determinant of intermediate temperature mechanical behaviour [20, 21]. However, these arguments explaining the above results remain somewhat inconclusive, because no direct observation supporting the exact strengthening mechanism has been available.

The effect of lattice mismatch is manifested through an inverse dependence between interfacial dislocation spacing and lattice mismatch [22]. As the lattice mismatch is increased, the interfacial dislocations become more closely spaced. As already mentioned, the lattice mismatch between γ and γ′ was increased from near zero to − 0.26% by the 3 wt % Re addition. Therefore, the interfacial dislocation density of 3Re alloy having a larger lattice mismatch may be higher than that of 0Re alloy. Externally applied load upon the creep test accelerates the formation of the interfacial dislocation network. The dislocation network that formed during the primary creep stage was stable and sessile structures which apparently strengthened interfaces by interacting with mobile dislocations [22].

Fig. 11 confirms the above explanation, which is consistent with the results presented by other investigators [20, 21]. One of the most prominent features in Fig. 11a is that there are many tangled dislocation structures in 3Re alloy indicating a strong interaction between the gliding dislocation and the interfacial dislocation. The tangled dislocation structure around γ′ particle acts as a more effective barrier for further

glide dislocation motion. Comparing with Fig. 11a, no tangled dislocation structure was observed in 0Re alloy, shown in Fig. 11b. For 0Re alloy having a near zero γ–γ' lattice mismatch, relatively small interaction between glide and interface dislocations is expected to occur due to the low interfacial dislocation density. This resulted in a weak γ–γ' interface formation, which may be one of the reasons for the lower creep rupture strength of 0Re alloy.

4. Conclusions

The influence of the 3 wt % Re addition on γ' morphology and intermediate-temperature creep strength can be summarized as follows.

1. The rhenium addition significantly retards γ' particle coarsening kinetics. This can be explained by the fact that rhenium acts as a rate-controlling species upon the volume diffusion-controlled coarsening process because rhenium is a heavy element and it almost solely partitions to the γ matrix. It was found that the activation energy for γ' particle coarsening increased by 38% upon 3 wt % Re addition. This supports the reduction of the particle coarsening rate of rhenium bearing alloy.

2. The magnitude of the lattice mismatch between γ and γ' increased from 0 to -0.26% at room temperature with the 3 wt % Re addition. This increased lattice mismatch for 3Re alloy causes the formation of more aligned and cuboidal γ' precipitates rather than random and irregularly shaped γ' precipitates observed for 0Re alloy.

3. The γ' morphological change due to the rhenium addition described above was responsible for two-fold improvement in creep life of 3Re alloy compared with 0Re alloy. This is presumably due to the change in the mode of precipitate–dislocation interaction. For 3Re alloy, mobile dislocations at γ–γ' interfaces must cut finer, more cuboidal and aligned γ' precipitates in order to proceed. Shearing of precipitates, as evinced by the existence of stacking faults, results in an increase in creep strength. However, lower creep strength was observed for 0Re alloy because a dislocation looping mode dominates with coarser and more irregularly shaped γ' precipitates.

4. Many tangled dislocation structures were observed in 3Re alloy having higher γ–γ' lattice mismatch value, which resulted from strong interaction between the glide dislocation and the interfacial dislocation. That may act as an effective barrier for glide dislocation motion, leading to an increase in the creep strength for 3Re alloy.

Acknowledgement

The authors acknowledge Inco Alloy International, Inc., for supplying the specimens.

References

1. H. F. MERRICK, L. R. CURWICK and Y. G. KIM, NASA CR-135150, January 1977 and NASA CR-159493, May 1979.
2. E. ARZT and L. SCHULTZ, in "New Materials by Mechanical Alloying Technique" (Deutsche Gesellschaft für Metallkunde, Oberursel, Germany, 1989) p. 28.
3. D. BLAVETT, P. CARON and T. KHAN, *Scripta Metall.* **20** (1986) 1396.
4. A. F. GIAMEI and D. L. ANTON, *Metall. Trans.* **16A** (1985) 1997.
5. I. M. LIFSHITZ and V. V. SLYOZOV, *J. Phys. Chem. Solids* **19** (1981) 35.
6. C. WAGNER, *Z. Elktrochem.* **65** (1961) 581.
7. J. ASKILL, in "Tracer Diffusion Data for Metals and Simple Oxides" (Plenum Press, New York, NY, 1970).
8. A. J. ARDELL, R. B. NICHOLSON and J. D. ESHELBY, *Acta Metall.* **14** (1966) 1295.
9. MINORU DOI and TORU MIYAZAKI, *Mater. Sci. Eng.* **78** (1986) 87.
10. MINORU DOI, TORU MIYAZAKI and TERUYUKI WAKATSUKI, *ibid.* **67** (1984) 247.
11. M. V. NATHAL and L. J. EBERT, *Metall. Trans.* **16A** (1985) 1849.
12. M .V. NATHAL, R. A. MACKAY and R. G. GARLICK, *Mater. Sci. Eng.* **75** (1985) 195.
13. D. A. PORTER and K. E. EASTERLING, in "Phase Transformations in Metals and Alloys" (Van Nostrand Reinhold Company, NY, USA, 1981) pp. 161–4.
14. R. A. MACKAY and M. V. NATHAL, *Acta Metall.* **38** (1990) 993.
15. C. K. L. DAVIES, P. NASH and R. N. STEVENS, *J. Mater. Sci.* **15** (1980) 1521.
16. C. T. SIMS, N. S. STOLOFF and W. C. HAGEL, in "Superalloy II" (J Wiley, NY, USA, 1987) pp. 66–78.
17. G. R. LEVERANT and B. H. KEAR, *Metall. Trans.* **1** (1970) 491.
18. B. H. KEAR, G. R. LEVERANT and J. M. OBLAK, *Trans. Am. Soc. Metals* **62** (1969) 639.
19. S. M. COPLEY and B. H. KEAR, *Trans. AIME* **239** (1967) 984.
20. M. V. NATHAL, *Metall. Trans.* **18A** (1987) 1961.
21. D. A. GROSE and G. S. ANSELL, *ibid.* **12A** (1981) 1631.
22. T. P. GABB, S. L. DRAPER, D. R. HULL, R. A. MACKAY and M. V. NATHAL, *Mater. Sci. Eng.* **A118** (1989) 59.

Received 4 March 1997
and accepted 22 April 1998